RESEARCH ARTICLE

High Data-Rate Hilbert-Curved-Shaped MIMO Antenna With Improved Bandwidth and Circular Polarization for Wireless Capsule Endoscopy

SYED MISBAH UN NOOR[1], SYED AHSON ALI SHAH[2], (Member, IEEE), SHAHID KHAN[3], IZAZ ALI SHAH[4], JAMAL NASIR[1], SALAHUDDIN KHAN[5], AND SLAWOMIR KOZIEL[3,6], (Fellow, IEEE)

[1]Department of Electrical and Computer Engineering, COMSATS University Islamabad, Abbottabad Campus, Abbottabad 22044, Pakistan
[2]Graduate School of Energy Convergence, Gwangju Institute of Science and Technology, Gwangju 61005, South Korea
[3]Faculty of Electronics, Telecommunications and Informatics, Gdańsk University of Technology, 80-233 Gdańsk, Poland
[4]Department of Electronic Engineering, Hanyang University, Seoul 04763, South Korea
[5]College of Engineering, King Saud University, Riyadh 11421, Saudi Arabia
[6]Engineering Optimization and Modeling Center, Reykjavik University, 101 Reykjavik, Iceland

Corresponding author: Slawomir Koziel (koziel@ru.is)

ABSTRACT The growing demand for wireless communication in biomedical engineering has opened new research frontiers. This paper introduces an innovative miniaturized (4×9 mm^2) multiple-input multiple-output (MIMO) circularly polarized (CP) implantable antenna for a wireless capsule endoscopy (WCE) system. The presented device features two Hilbert curve-shaped meandered resonators. The space-filling characteristic inherent in the Hilbert curve contributes to miniaturization and bandwidth enhancement of up to 250 MHz to cover possible detuning between diverse organs. Simultaneously, employing the curve's inherent natural symmetry and adopting an orthogonal port arrangement led to a noteworthy improvement in isolation up to 27 dB with an enhanced gain of -27.9 dBi. Comprehensive simulation analysis of antenna-integrated WCE systems in homogeneous and hetrogenous environments is conducted in the stomach, small intestine, and large intestine. Without the need for an external decoupling structure, the system demonstrated good MIMO characteristics with isolation of 27 dB. A fabricated prototype has been tested in a saline solution and minced pork. A good match between the measured and simulated results has been observed. At both ports, the axial ratio ($<$ 3 dB) covers part of the ISM band in the homogeneous stomach, small intestine, and large intestine phantoms. Additionally, a safety assessment, employing a realistic human model, aligns findings with established safety guidelines, revealing average specific absorption rates of 543 W/kg (1 g) and 58.6 W/kg (10 g) at 2.45 GHz. Moreover, link budget analysis confirms reliable wireless data transmission up to 1.8 m at 78 Mbps. The proposed MIMO antenna, with its superb dominant characteristics, outperforms leading state-of-the-art endoscopic antennas, offering promising advancements for capsule endoscopy systems.

INDEX TERMS MIMO antenna, endoscopic antenna, high data rate, biomedical antenna, Hilbert.

I. INTRODUCTION

Wired medical devices, despite their clinical utility, pose inherent restrictions. Limited communication range, patient

The associate editor coordinating the review of this manuscript and approving it for publication was Hassan Tariq Chattha.

discomfort due to tethering, and reduced activity levels necessitate a paradigm shift toward wireless solutions. Consequently, research and development efforts have pivoted towards the innovative frontiers of wireless medical technology [1], [2]. Wireless biomedical telemetry systems are capable of early disease detection, and diagnosis precise,
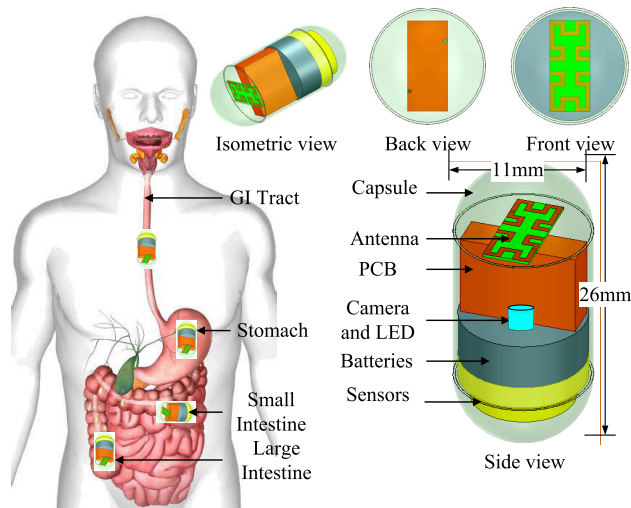
FIGURE 1. Overview of the MIMO antenna integrated WCE System.

real-time monitoring and targeted therapeutic interventions [3], [4]. These systems have the potential to reshape the medical landscape across diverse domains, including cardiac, neuromodulatory, endoscopic, ophthalmic, and glucose monitoring [2], [5], [6], [7], [8], [9]. Wireless biomedical telemetry facilitates accurate measurement of physiological signals in ambulatory patients, enabling continuous monitoring and data acquisition while preserving their mobility. This technological breakthrough empowers both hospital resource optimization and patient care enhancement, ultimately leading to improved healthcare accessibility for all [10].

Traditional wired endoscopes face difficulties in navigating the twisted large intestine. To address this limitation, WCE emerged as a revolutionary modality capable of comprehensively examining the entire gastrointestinal (GI) tract, as detailed in [11]. The core purpose of WCE lies in aiding clinicians in accurately identifying and effectively treating digestive system diseases. This is achieved by utilising commercially available capsule devices designed explicitly for GI endoscopic exploration. Enclosed within a compact 11 mm × 26 mm shell, the WCE capsule houses several crucial components: an optical dome, battery system, camera, light-emitting diodes (LEDs), sensors, and most importantly, an antenna [12], [13], [14] as shown in Fig. 1. The antenna serves as the critical communication channel between the external base station and the capsule, enabling wireless data transmission throughout the examination process. Because the environment surrounding the human body is so dynamic and complicated, WCE antenna design presents major difficulties. The electrical properties of the GI tract exhibit significant inter-organ variation, leading to dynamic shifts in the antenna's impedance matching as it navigates the GI tract, adversely affecting its performance. Moreover, WCE's small dimensions and high data transfer requirements further increase the complexity of the antenna design [2], [15].

The development of an endoscopic antenna requires a design with a broad bandwidth, high data rates, and small size. MIMO technology, which uses multiple antennas on the transmission and reception ends, is useful to meet these needs. According to recent research, MIMO-embedded antennas exhibit higher spectral efficiency. Comparing such MIMO antenna systems to single-input single-output (SISO) antenna systems, enhaned channel capacity is possible without requiring an increase in power or bandwidth use. The MIMO technique therefore has the potential to attain large data rates in applications involving medical implants [12]. Recent research has proposed many types of implantable antennas that suit the requirements of compactness, proper radiation characteristics, safety concerns, and consistent connection performance [16], [17], [18]. On the other hand, these solutions use a SISO architecture. Nevertheless, SISO antennas are not able to meet the demands for high data throughput and spectral efficiency.

Recent demonstrations have underscored the superior suitability of MIMO systems over SISO systems for achieving elevated throughput gains in capsule endoscopic applications [11], [19]. In [20], researchers suggested a more compact four-element MIMO implantable antenna that functions at the 2.45 GHz ISM frequency and has a volume of $18.5 \times 18.5 \times 1.27$ mm^3. A cross-shaped slot etched in the radiator, a branch extending on the conductor ground, and a pair of electromagnetic band gaps (EBGs) are integrated to achieve a high isolation of 15.99 dB isolation. A dual antenna system with enhanced isolation operating at 2.45 GHz ISM band and volume of $10.5 \times 10.5 \times 0.635$ mm^3 for bio-telemetry application is presented in [21]. Thereafter the inter-element isolation of the antenna system is significantly improved by 37 dB by employing the neutralization line between the two radiating elements and defected ground structure. Moreover, an implantable 3D MIMO antenna operating at 2.45 GHz for biotelemetry applications is developed in [22]. Nevertheless, despite the system's impracticality for insertion into a capsule with large cube dimensions of $15 \times 15 \times 15$ mm^3 for implantable antennas, the design offers benefits like polarization and 3D orientation insensitivity. A two-element MIMO antenna setup intended for 2.45 GHz wireless capsule endoscopy was presented in an earlier paper [23]. This antenna exhibited a wide bandwidth, strong isolation, and high data rates. The antenna's small size of $5 \times 4.2 \times 0.12$ mm^3 was made possible by the use of meandering geometry, a defective ground structure, and a high permittivity substrate. This combination of factors led to a -30 dB reduction in mutual coupling between the antennas. Another study in [24] proposed an implanted antenna for deep tissue implantation consisting of two 2.45 GHz MIMO elements. The antenna was sized $5.35 \times 6.2 \times 0.12$ mm^3 and achieved 28 dB isolation and 320 MHz bandwidth using vertical gaps in the ground layer. In a previous study [25], the authors proposed a small dual-band MIMO antenna with two ports for effective data transmission into deep tissue. Operating

in the 915–2450 MHz Industrial, Scientific, and Medical (ISM) bands, the MIMO antenna's measured bandwidth was 148.5 MHz. Its small size of $10.8 \times 5.6 \times 0.254$ mm^3 was made possible by the addition of two ground plane slots and meandered resonators.

Hilbert curves can be densely packed into a compact area while preserving a long electrical length, making them ideal for applications like wireless capsule endoscopy where space is constrained. Additionally, Hilbert curve-shaped antennas exhibit low mutual coupling due to current cancellation, making them beneficial for use in MIMO systems. Hilbert curve-shaped antennas have been proposed in the literature, leveraging the advantageous characteristics of the hilbert curve. A MIMO conformal two-port Hilbert third iteration antenna is presented in [26] with an area of 13×6 mm^2. However, the design has certian drawbacks, including lack of optimization for achieving circular polarization, which is a requirement for WCE systems. Additionally, using the third iteration makes the design bulkier and more complex, resulting in a bandwidth larger than necessary for the desired 2450 MHz ISM band. The antenna is conformal in shape making it difficult for fabrication on the respective substrate. The design also has a low gain of -41.8 dBi at 2450 MHz. Another antenna using the Hilbert shape is presented in a conformal design, making fabrication challenging [27]. This antenna employs the third iteration of the Hilbert curve with three interconnected elements. It is a SISO antenna with a low data rate, and it lacks optimization for achieving circular polarization characteristics.

The choice between 400 MHz and 2.45 GHz for endoscopic antennas depends on the application's specific requirements. 400 MHz provides better tissue penetration and longer communication range but suffers from lower antenna efficiency due to its longer wavelength $\lambda \approx 75$ cm, limiting miniaturization. In contrast, 2.45 GHz offers more compact antenna designs $\lambda \approx 12.5$ cm and higher data rates, making it suitable for applications where size and throughput are critical, though it experiences higher attenuation in biological tissues, necessitating closer proximity. Additionally, 2.45 GHz enables easier transition from SISO to MIMO designs due to the smaller antenna size.

It is important to realize that a completely grounded arrangement cannot provide total port isolation without a decoupling technique. Despite significant progress in MIMO antenna design for implanted applications, limitations remain across studies. Notably, achieving sufficient isolation and a high axial ratio (AR) performance between antenna elements while keeping the size acceptable for capsule endoscopy or deep tissue implantation proves challenging. This trade-off between isolation, AR performance, and miniaturization restricts the widespread adoption of MIMO technology in these areas. The novelty of our design lies in intelligently using the second iteration of the Hilbert curve to create a less complex structure. Additionally, a current cancellation technique is employed to reduce mutual coupling, and optimization has been performed to achieve circular polarization

features. This design is also miniaturized compared to other Hilbert curve antennas. From a detuning perspective, our design resonates within the ISM band in the stomach, small intestine, and large intestine. These features and circular polarization characteristics make the design novel and useful for the target wireless application.

This paper proposes a comprehensive solution to address issues related to compactness, circular polarization (CP) performance, and the achievement of high data rates within a compact-sized design. A dual-port miniaturized MIMO CP Hilbert curve design having compact dimensions of $4 \times 9 \times 0.5$ mm^3 is proposed for WCE applications in the ISM 2.45 GHz band. To reduce the antenna size, the proposed MIMO antenna utilizes the fractals of the Hilbert curve. On the other hand, vias which are commonly employed in the miniaturization of implantable antennas are avoided thereby making the design fabrication easy and low-cost. Furthermore, the suggested design uses orthogonal placements of the feeding pins which not only helps in achieving CP but also results in reduced mutual coupling without the use of any additional mutual coupling compensation structures. The performance of the proposed MIMO CP implantable antenna has been evaluated in terms of antenna parameters (S-parameters, radiation patterns, SAR, link margin) and MIMO parameters (ECC and DG). These parameters were found to be within the acceptable ranges. To the best of the authors' knowledge, the proposed design is the first compact CP-based MIMO design proposed for WCE applications. Compared to existing MIMO implantable antennas, the proposed design exhibits a significantly smaller footprint while maintaining acceptable mutual coupling. Notably, it achieves desirable characteristics without resorting to conventional mutual coupling reduction strategies, such as ground plane slot etching, metal via integration, or metamaterial implementation, which leads to considerable complexity in the fabrication and implementation process. Due to deploying the Hilbert structure, both orthogonal ports of MIMO exhibit an AR of less the 3 dB at the ISM band in the stomach, small intestine, and large intestine.

II. DESIGN METHODOLOGY
A. SIMULATION AND MEASUREMENT SETUP
The specific simulation environment, as depicted in Fig. 2 utilizes standard electromagnetic simulation tools, including Sim4Life (Fig. 2(b)) and Ansys HFSS (Fig. 2(d)), to characterize the proposed antenna performance. The simulation environment for implantable antennas significantly differs from that of free-space antennas, as implantable antennas are designed to operate within a tissue or human phantoms. To ensure accuracy, the simulation parameters are set for terminal mode operation at 2.45 GHz, with a maximum of 20 passes, a convergence criterion of 0.01, and a frequency sweep ranging from 2.2 to 2.8 GHz in 1 MHz increments. No additional specific conditions, beyond the standard settings recommended in the user manuals of these tools, were applied [24]. Sim4Life software has the potential to
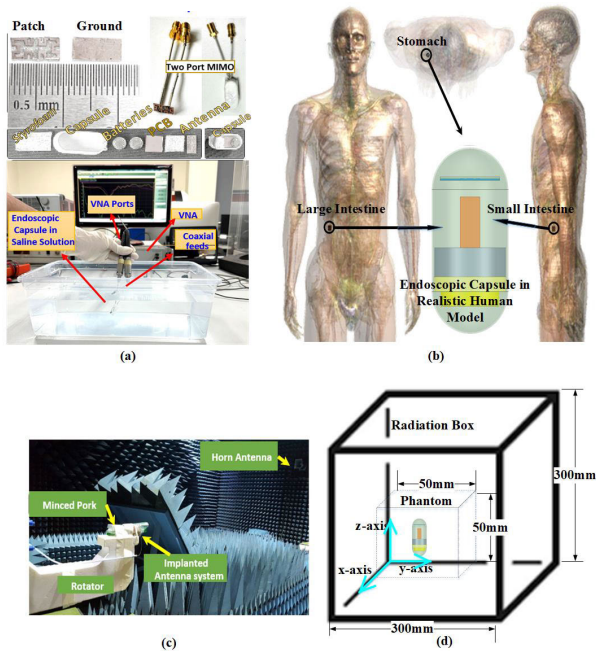
FIGURE 2. Performance analysis of the MIMO WCE system: (a) Experimental validation of fabricated prototypes for $|S_{11}|$ measurement; (b) Heterogeneous environment (Sim4life); (c) Gain and radiation pattern measurements in the anechoic chamber; (d) Homogeneous environment (HFSS).

replicate the same environment as a human organ. For the HFSS simulation environment, we create a hollow capsule simulation in HFSS by configuring its parameters to resemble 9.8 alumina with a 0.2 mm thickness. Frequency-dependent homogeneous tissue phantoms representing the stomach, small intestine, and large intestine, each measuring $50 \times 50 \times 50$ mm^3, were utilized in HFSS, with the antenna positioned at the centre of the phantom (at a depth of 25 mm). A radiation box measuring $300 \times 300 \times 300$ mm^3 in HFSS was employed to optimize the proposed MIMO antenna system, as shown in Figure 2(d). The human organs in HFSS have been simulated with a homogenous environment. The relative permittivity values used for the stomach small intestines and large intestines were 62.2, 54.4, and 53.8, respectively with conductivity values of 2.21, 3.17, and 2 S/m at 2.45 GHz. To create a realistic capsule more dummy parts for the capsule, such as batteries, circuit boards, sensors, LEDs, and a camera are incorporated. The MIMO antenna was placed within an endoscopic capsule device across a variety of tissues in Sim4Life to evaluate its performance in a heterogeneous environment.

To verify the simulation results, an experimental validation (fabrication and measurement) of the intended two-port MIMO antenna was conducted on a fabricated prototype using a 0.25 mm Rogers RO3010 substrate with a dielectric constant of 10.2 and a loss tangent of 0.002. The aluminium (Al2O3) material with a relative permittivity of 9.8 and a thickness of 0.2 mm measuring was used to enclose the 3D printed capsule to make it bio-compatible. It is

essential to mimic the capsule's architecture for precise results. To practically mimic the PCB, camera LED, and two sensors, Roger RT/duriod 3010 material was used, whereas for batteries, PEC was used in the simulation as shown in Fig. 2(b).

For practical validations, measurements of S-parameters and radiation patterns were conducted using a vector network analyzer (VNA) within a container filled with a saline solution and minced pork, respectively. The experimental validation is limited to saline solution and minced pork, which although do not mimic the exact properties of the human gastrointestinal tract, however as an alternative, we must emulate conditions similar to those associated with human anatomy. To carry out more realistic and diverse testing environments, we need patient permission and legal procedures, which are usually required at the stages of technology commercialization. During the stages of research, researchers, designers, and practitioners typically adopt alternative standardized procedures that produce similar results as that of the human body. To verify the performance of implantable antennas, the economical and accurate way is to use human mimicking phantom, saline solution, minced pork, minced meat, and other customized phantoms. Therefore, in our study, we have followed the same standardized experimental protocols to evaluate the performance of the antenna i.e. saline solution for S-parameters and minced pork for radiation pattern. For gain pattern, saline solution is not used as there is a risk of saline leakage and spill-off due to rotator rotation for the pattern measurements in the H- and E-planes. To create phantoms that mimic the relative permittivity of the stomach (permittivity: 62.2, conductivity: 2.21 S/m) at 2.45 GHz, a solution is prepared by adding 25.5% sugar and 0.01% NaCl by weight to distilled water. This formulation effectively simulates the dielectric properties of human tissue, with the dielectric characteristics of the mixture remaining stable for several days, even without preservatives [28]. The findings have shown that the proposed antenna has consistent performance in different environments, with a good agreement between the simulation and experimental results, thereby demonstrating the efficacy of design and validations. The S-parameters of the fabricated antenna were evaluated in saline solution, as depicted in Fig. 2(a). This includes S-parameter measurements in a saline solution and gain measurements in minced pork, which are typically used to test the practical performance of an implantable antenna [3], [5], [7], [14]. During the measurements, the implantable antenna along with other components was placed in the capsule device. The standard experimental procedures were then followed to obtain the results. Typically, S-parameters are measured using a VNA, where the coaxial feed ports from the VNA are connected to the coaxial feed ports of the antenna. For gain pattern measurements, the antenna is placed on the rotator in an anechoic chamber room, where the standard procedures for gain pattern measurement are implemented [29]. The evaluation of the radiation pattern in terms of E- and H-planes
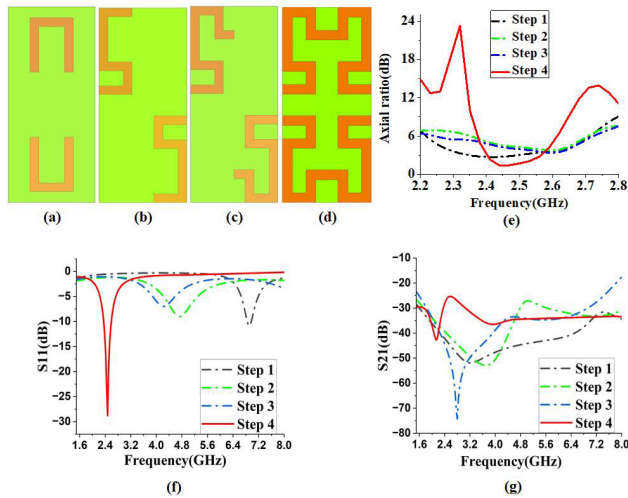
FIGURE 3. Steps of the proposed design (a) Step 1 (b) Step 2 (c) Step 3 (d) Step 4 (e) axial ratio of design steps (f) $|S_{11}|$ of design steps (g) $|S_{21}|$ of design steps.

involved a spectrum analyzer, a high-gain horn antenna, and a signal generator, as illustrated in Fig. 2(c). The high-gain horn served as the transmission source, while the implanted antenna acted as the receiver. A three-meter distance was maintained between the recommended antenna and the edge of the horn antenna. For radiation pattern measurement the proposed implantable antenna was rotated in 5-degree increments to capture the power in the E and H planes.

B. DESIGN EVOLUTION OF THE PROPOSED MIMO ANTENNA

The proposed design undergoes finalization through a systematic four-step process. Firstly, a level 1 Hilbert curve is established as the foundational framework. Subsequently, the meandering structure is constructed on the substrate, enabling the antenna to operate at lower frequencies. The determination of the resonator's length is facilitated by equation (1), which is employed for accurate calculations.

$$L_{\text{sr}} = \frac{c}{2f\sqrt{\varepsilon_{\text{r}}}} \tag{1}$$

where L_{sr} denotes the effective length of the meandering radiator, f represents the operating frequency, and c is the speed of light. The estimated resonator length (L_{sr}) measures 19 mm at 2.45 GHz. In Step 1, resonance occurs at 7.2 GHz with a simple U-shaped 1st-level Hilbert curve, as illustrated in Fig. 3(a). To further extend the length, a portion of the 2nd-level Hilbert curve is incorporated in Step 2. Additional segments are integrated into the 2nd-level Hilbert curve, resulting in resonance at 4.8 GHz, depicted in Fig. 3(b) In the Step 3, the meandered patch length is augmented by incorporating a portion of the 2nd-level Hilbert shape, causing the resonance frequency to decrease from 4.8 GHz to 4 GHz, as shown in Fig. 3(c). Upon completion of the 2nd level Hilbert curve in the Step 4,
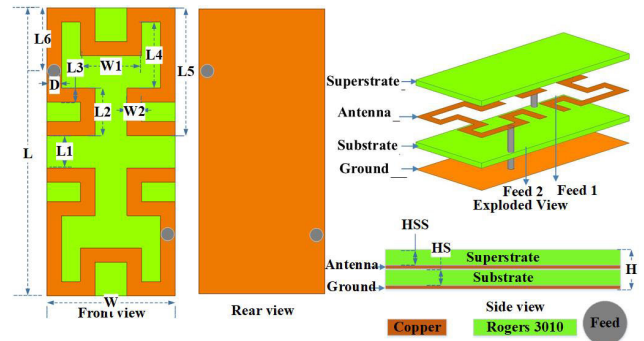
resonance frequency decreases to the desired 2.45 GHz, achieving resonance within the ISM band, as illustrated in Fig. 3(d). U-shaped curve, the basic structure can be described mathematically in terms of a set of linear segments connecting points. This simple curve is the foundation for higher-order Hilbert curves, which become increasingly complex through recursive subdivision. Increasing the order allows for greater length and current path, which in turn achieves the size miniaturization and the desired band.

Each of the aforementioned steps exhibits reflection coefficients of −12 dB, −9 dB, −7 dB, and −29 dB, respectively, as depicted in Fig. 3(f). At approximately 2450 MHz, the frequency demonstrates good impedance matching with a reflection coefficient of −29 dB and a bandwidth of 250 MHz in the final proposed Step 4. Isolation between ports in each step, shown in Fig. 3(g), reveals $|S_{21}|$ consistently below −27 dB at 2.45 GHz. Additionally, CP performance in each step, as depicted in Fig. 3(e), demonstrates incremental improvement, with Step 4 achieving the best CP performance within the desired ISM band. Antenna design steps give an idea of the optimization for the antenna design parameters and explain the trade-offs among the performance metrics.

FIGURE 4. Geometry of the proposed MIMO antenna with front view, rear view, exploded view, and side view.

TABLE 1. Antenna parameters.

Parameter	Value mm	Parameter	Value mm
W	4	L6	2
L	9	W1	1.9
L1	1	W2	0.45
L2	1.5	D	0.15
L3	0.45	HS	0.25
L4	2.05	HSS	0.25
L5	4	H	0.5

C. PROPOSED MIMO ANTENNA DESIGN CONFIGURATION

Fig. 4 depicts the size and geometric layout of the proposed antenna, showcasing both the top and bottom perspectives of the ground plane along with depictions of the radiating patch. The substrate used in the design was 0.127 mm thick Rogers RT/duroid 3010 with a dielectric constant of 10.2 and a loss factor (tanδ) of 0.0022. A 0.25 mm-thick Rogers RT/duroid
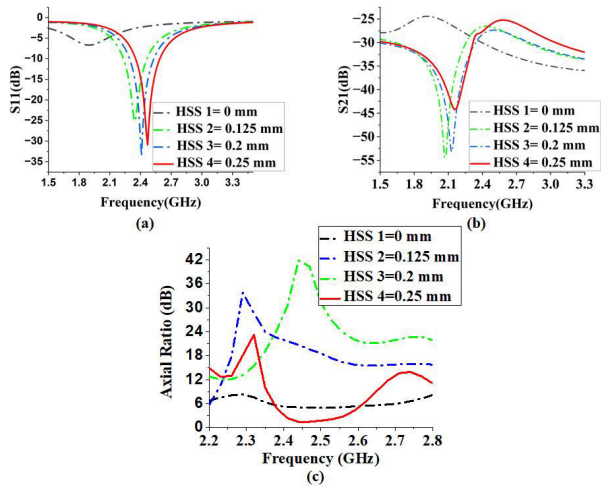
FIGURE 5. Impact of superstrate height (a) $|S_{11}|$ (b) $|S_{21}|$ (c) axial ratio.

FIGURE 6. Impact of Hilbert width (a) axial ratio (b) $|S_{11}|$ (c) $|S_{21}|$.

FIGURE 7. Impact of feed position (a) axial ratio (b) $|S_{11}|$ (c) $|S_{21}|$.

3010 material is used, which acts as a superstrate to support the radiating patch and enhance bandwidth as well as the gain of the proposed antenna. The Hilbert Curve with a width of 0.15 mm is easily etched through a conventional etching mechanism or through a laser etching mechanism. The number of Hilbert curve does not matter for both the etching mechanisms. The overall dimensions of the antenna are $4 \times 9 \times 0.5$ mm^3, whose parameters are summarised in Table 1. For the excitation of the proposed MIMO antenna two 50 Ω coaxial probes having inner conductor and outer dielectric cable diameters of 0.25 and 1.5 mm, respectively were used. Both the elements of the presented MIMO antenna were kept at a separation (L1) of 1 mm. Due to the meandered nature of the proposed antenna the currents flowing on the unexcited elements can be made to cancel resulting in high isolation without the need of any decoupling structure.

III. PARAMETRIC STUDY AND ANALYSIS

This section outlines the tuning method and impedance matching of the proposed antenna. To facilitate customization of the antenna's adaptive parameters for specific objectives, a parametric analysis is conducted to ensure optimal performance. The suggested antenna undergoes examination through a parametric study involving four parameters, which are discussed in detail below.

A. EFFECT OF SUPERSTRATE THICKNESS

Adjusting the thickness (HSS) makes it easy to match and tune the antenna to the designated bands, as depicted in Fig. 5(a). In the absence of a superstrate, the resonant frequency is observed at 1900 MHz with mismatching. The introduction of a 0.2 mm thick superstrate, composed of the same material as the substrate, shifts the resonance frequency to 2400 MHz. A 0.25 mm thick layer of superstrate is added to obtain the desired frequency, giving the substrate and superstrate a combined thickness of 0.5 mm. $|S_{21}|$ plots in Fig. 5(b) demonstrate that different superstrate thicknesses
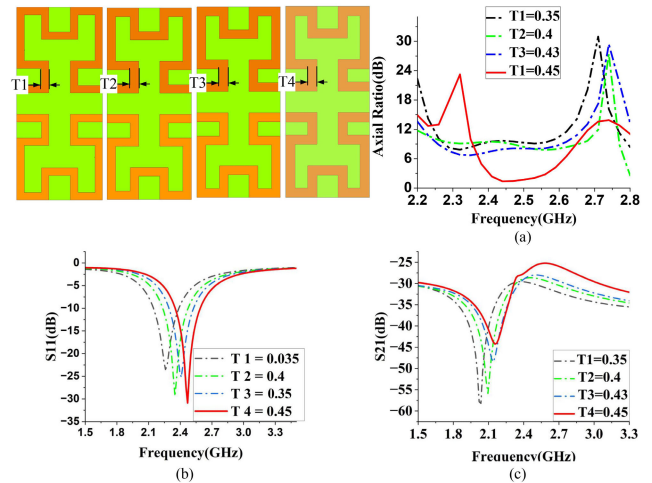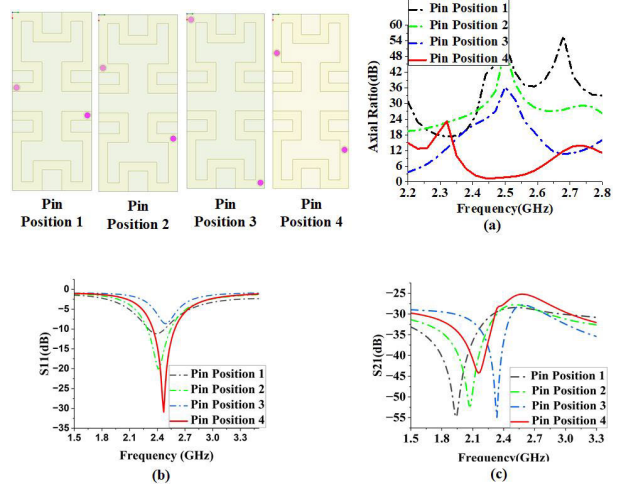
impact isolation between ports minimally. Similarly, Fig. 5(c) illustrates the significant effect of superstrate thickness on the CP performance of the proposed antenna. Optimal CP performance is attained with a superstrate thickness (HSS) of 0.25 mm. Fig. 5 underscores that a superstrate with 0.25 mm thickness performs optimally, justifying its utilization in the proposed design.

B. EFFECT OF HILBERT WIDTH

The variations in the width of the Hilbert-shaped radiator were explored to assess the antenna's performance in terms of resonant frequency shifting, as depicted in Fig. 6(b). This illustrates that the resonant frequency shifts towards the higher end of the frequency spectrum with increasing width. The width of the Hilbert-shaped strips denoted as T1, T2, T3, and T4, are sequentially 0.35 mm, 0.4 mm, 0.43 mm, and 0.45 mm. Upon closer examination of the $|S_{21}|$ graph in Fig. 6(c), it becomes evident that as the width of the Hilbert strip increases from 0.35 to 0.45 mm, there is a slight decrease in port isolation.
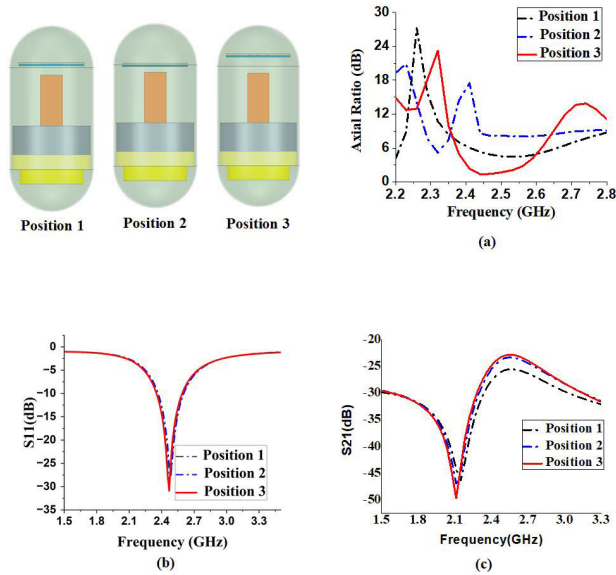
FIGURE 8. Impact of capsule position (a) axial ratio (b) $|S_{11}|$ (c) $|S_{21}|$.
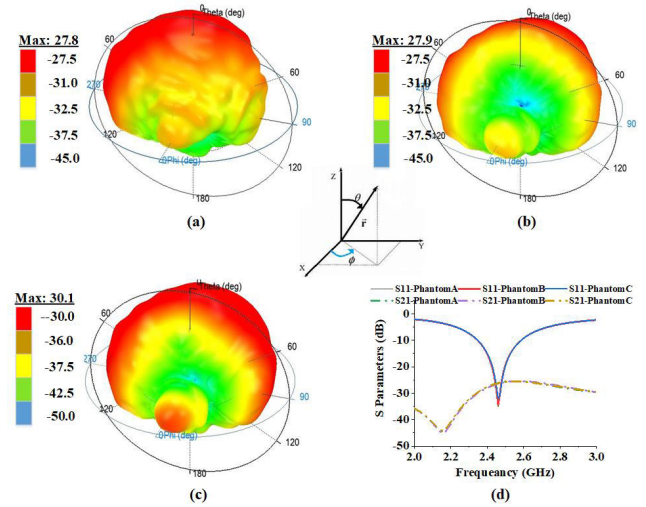

FIGURE 9. Proposed MIMO antenna (a) Simulated S-parameters for Phantom A, Phantom B, and Phantom C (b) Simulated 3D radiation patterns in Phantom A (c) Simulated 3D radiation patterns in Phantom B (d) Simulated 3D radiation patterns in Phantom.

The impact of strip width on the CP performance of the proposed antenna is depicted in Fig. 6(a). It is discernible from the figure that as the strip width increases, the AR in the desired band improves, reaching the desired value (below 3 dB) when the strip width is T4= 0.45 mm. Fig. 6 underscores that a width of T4= 0.45 mm performs optimally, justifying its utilization in the proposed design.

C. EFFECT OF FEED POSITION

One of the most important factors affecting the impedance matching at the defined frequency bands is the feeding point's location. The impact of the feeding pin position is shown in Fig. 7. In Fig. 7(b) shifting pin locations on the Hilbert curve affect the resonating frequency's matching. The $|S_{21}|$ graph in Fig. 7(c) shows the feed's placement has a substantial impact on the mutual coupling between ports. There is a similar reduction in mutual coupling as port separation grows. Port locations must be adjusted to obtain optimal matching. Similarly, the effect of port location on the CP performance of the proposed antenna is given in Fig. 7(a). The figure reveals that changing the port locations changes the AR significantly and Pin Position 4 gives the desired AR in the targeted band. It is found that pin position 4 is the ideal pin location for this suggested design.

D. EFFECT OF ANTENNA POSITION INSIDE THE CAPSULE

The endoscopic antenna is a crucial part of WCE functioning in tandem with other electronic components such as a printed circuit board (PCB), light-emitting diodes (LEDs), cameras, and batteries. These parts are included in the IMD, usually with the antenna at the very top. It is essential to assess how these components affect the antenna's performance. As given in Fig. 8, Parametric research was carried out to look into this, where the antenna's location inside the capsule was systematically changed. The alteration of the antenna position within the capsule has a negligible impact on port isolation, as indicated by the $|S_{21}|$ parameter in Fig. 8(b). Likewise, the effect of antenna position inside the capsule affects its CP performance. "Position 3" in Fig. 8 (a)gives the optimum AR due to the reduced coupling effect of the other components on the antenna.

E. EFFECT OF VARIATION IN PHANTOM ANATOMY

The impact of varying patient populations is modelled in HFSS through alterations in phantom sizes, accounting for differences in human anatomy and physiology. Fig. 9 shows the reflection coefficients and gain of the proposed design in different phantoms. These three phantoms, $40 \times 40 \times 40$ mm^3 (Phantom A), $50 \times 50 \times 50$ mm^3 (Phantom B), and $60 \times 60 \times 60$ mm^3 (Phantom C) represent three different humans with varying body sizes. Phantoms A, B, and C have antennas positioned at depths of 20 mm, 25 mm, and 30 mm, respectively. The simulated S-parameters exhibit minimal changes in the three phantoms (Phantom A, Phantom B and Phantom C) as shown in Fig. 9(d). Similarly, the 3D gain patterns exhibit slight variations in terms of gain in Phantom A, B, and C, as shown in Fig. 9(a), (b), and (c). The observed simulated gains in Phantom A, B and C are -27.8, -27.9 and -30.1 dBi, respectively. These figures show that the antenna's performance remains largely unaffected across diverse patient groups, including variations in gender, body weight, and age.

IV. RESULTS AND DISCUSSION
A. ANTENNA PARAMETERS
The antenna performance is characterized here using several factors, such as S-parameters, gain, radiation pattern, current distribution, polarization, specific absorption rate, and link budget analysis.
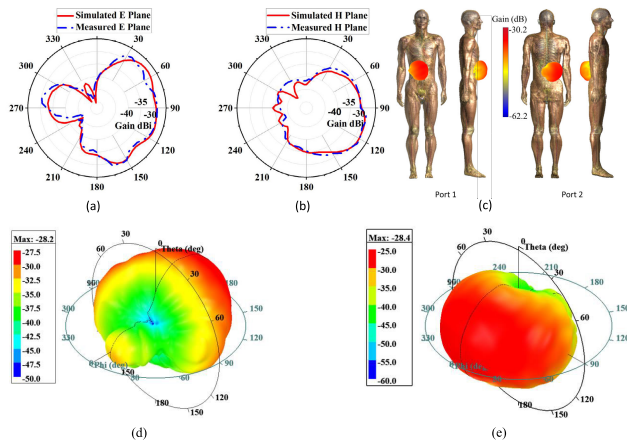
FIGURE 10. Proposed antenna (a)-(b) 2D simulated and measured radiation pattern in E and H-planes (c) Simulated 3D pattern in heterogeneous environment (sim4Life) (d)-(e) Simulated 3D pattern in homogeneous environment (HFSS).

1) GAIN AND RADIATION PATTERN

Measurements of gain and radiation patterns were conducted in minced pork to evaluate the suggested MIMO antenna's radiation properties. The receiving antenna was a horn antenna as discussed in Section II-A. The separation between the transmitting (Tx) and receiving (Rx) antennas was three meters to guarantee that each antenna was placed inside its designated far-field zone 2(c).The simulated and measured radiation patterns in the E and H-planes ($\theta = 0°$ and $\phi = 90°$) at 2.45 GHz are shown in Fig. 10(a)-(b). Similarly, the 3D pattern of the proposed antenna in a heterogeneous environment (Sim4Life) is presented in Fig. 10(c) showing a gain of -30.2 dBi. Likewise, the simulated 3D patterns of the presented antenna in homogeneous environment (HFSS) are shown in Fig. 10(d)-(e) for port-1 and port-2, respectively. It is clear from Fig. 10(d)-(e) that both ports of the proposed antenna having gains of -28.2 dBi and -28.4 dBi at 2.45 GHz are radiating in different directions hence satisfying pattern diversity which is required for increased coverage and reliable communication in a MIMO system. Fig.10(c) shows the behavior of radiation pattern at both ports. As can be noted, the radiation is directed outward. Note that physically the size of radiation is not like the one shown in the illustrative figure. It is merely a representation of the power flow direction.

2) SCATTERING PARAMETERS

Fig. 11 shows the measured and simulated S-parameters ($|S_{11}|$ and $|S_{21}|$). The proposed antenna exhibited isolation greater than 27 dB and resonance at 2.45 GHz with a fractional bandwidth of 250 MHz. Specifically, $|S_{11}|$, $|S_{22}|$ and $|S_{21}|$, $|S_{12}|$ were identical. The simulated $|S_{11}|$ and $|S_{21}|$ in the stomach, small intestine, and large are shown in Fig. 11(a) which covers most of the ISM band hence detuning is controlled. The simulated S-parameters in homogeneous (HFSS) and heterogeneous (Sim4Life) and measured (saline solution) are shown in Fig. 11(b). The homogeneous,
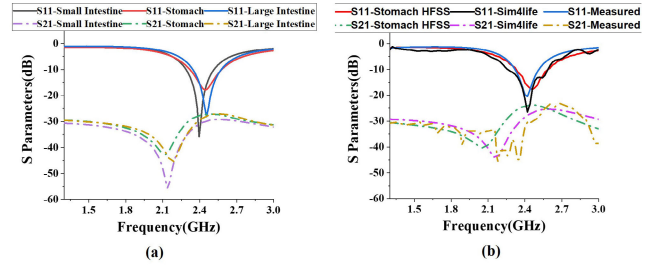

FIGURE 11. (a) S-Parameters in digestive system organs (b) simulated and measured S-Parameters.
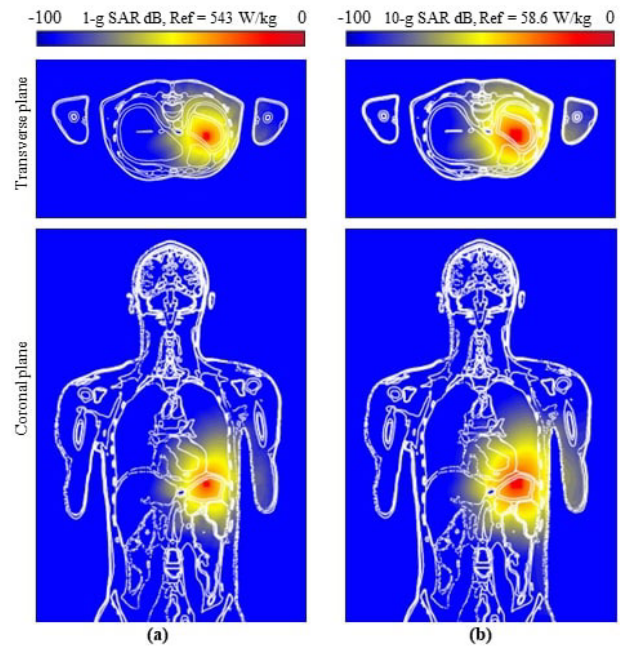

FIGURE 12. SAR distribution in a realistic human body model (Duke) (a) 1-g and (b) 10-g.

heterogeneous and measured $|S_{11}|$ are $-19, -22$ and -28 dB respectively at 2.45 GHz. The homogeneous, heterogeneous and measured $|S_{21}|$ are $-27, -29$ and -30 dB at the target frequency.

3) SPECIFIC ABSORPTION RATE (SAR)

SAR measures the rate at which electromagnetic radiation is absorbed by the human body per unit mass when exposed to an electromagnetic field. SAR is expressed in watts per kilogram (W/kg). During WCE, photos and videos of the GI tract are taken and transmitted to a distant receiver as electromagnetic radiation. Prolonged exposure to this radiation in humans can lead to tissue damage. The SAR equation illustrates the influence of mass density (ρ), conductivity (σ), and the strength of the electric field (E) on the SAR value [30].

$$\text{SAR} = \frac{\sigma E^2}{\rho} \qquad (2)$$

The electric field strength can be derived from power density using $|E| = \sqrt{\frac{S}{Z_0}}$, with S representing power density

and Z_0 being the characteristic impedance of free space. Additionally, SAR can be averaged over time to account for time-varying fields, expressed as $\text{SAR}_{\text{avg}} = \frac{1}{T} \int_0^T \text{SAR}(t)\, dt$.

As the electric field intensity increases, SAR also increases. Tissues with higher electrical conductivity and permittivity tend to absorb more electromagnetic energy, resulting in higher SAR values. Conversely, SAR decreases as tissue mass density increases. Additionally, increasing the distance from the radiation source leads to energy dispersion and a decrease in SAR values. Human tissues exhibit greater conductivity, and electric field intensity is lower at higher frequencies than at lower frequencies. To ensure human safety, the input power and SAR are crucial. To comply with IEEE C95.1-1999, the average SAR values across 1 g and 10 g of tissue must not exceed 1.6 W/kg and 2 W/kg, respectively [31], [32]. We performed simulations using the realistic human model in Sim4Life to evaluate the SAR of the suggested endoscopic two-port MIMO antenna within the stomach. The average SAR values for 1 g and 10 g at 2.45 GHz were found to be 543 W/kg and 58.6 W/kg, respectively, with the antenna's input power set at 1 W. In addition, the maximum available input power at 2.45 GHz for 1 g and 10 g SAR is 2.9 and 34.1 mw, respectively. For WCE, the input power is limited to 0.025 mW [25], [33]. From a calculation standpoint, 1 watt of power is applied to the antenna. As given in Fig. 12 our analysis in the stomach indicates that the proposed antenna adheres to safety standards, demonstrating no health risk to the user due to minimal electromagnetic energy absorption by the body. Moreover, the inward and outward direction of power has same effect in terms of SAR as the power originates from the same location. Fig. 12 shows the SAR which depends on the power absorbed by the tissues. Both ports radiate same amount of power, therefore, the SAR is same for both ports. Due to redundant and repetitive SAR figure, we intentionally omitted it as it carries no meaning since the information can be easily inferred from Fig. 10(c), 10(d), and 10(e) as well as Equation (2).

4) LINK BUDGET ANALYSIS

To ensure the effective transmission of biological data, it is imperative to ascertain the telemetry range between the external base station and the implanted device. In this study, a dipole antenna with a gain of 2.15 dBi was employed as the receiving antenna, while the proposed MIMO implanted antenna functioned as the transmitting antenna within the large intestine, stomach, and small intestine. The gains for these respective scenarios were determined to be -28.2 dBi, -29.2 dBi, and -30.1 dBi. Here we can see that the lowest gain is of the small intestine so the link budget calculations are performed only in small intestine.

Because of energy absorption, diffraction, dispersion, and reflection of electromagnetic fields, there is more complexity in the communication channel between the external device and the endoscopic antenna. To determine the effective

communication distance and clarify how the endoscopic antenna works, it is necessary to analyze the communication link. Although most implanted antennas have a transmitter power (Pt) limit of 25 μW, in the context of WCE, the transmitter power is directly proportional to the data rate and therefore greatly influences the overall system performance. When it comes to WCE, Lithium-ion (Li-ion) batteries are favoured due to their high energy density and lightweight properties, enabling them to meet size and weight constraints. These attributes are essential for minimizing the bulk and overall dimensions of the capsule. Typically, Li-ion batteries have a nominal voltage of 3.7 volts (V) and a common capacity of 55 mAh, which is the prevalent power source for capsules. These batteries are capable of powering a capsule for eight to ten hours. As these implantable antennas are for one-time use and this much power is more than enough for one one-time procedure. [25]. These batteries can run a capsule for eight to ten hours. Usually, this setup results in a 20 mW power transfer. In the present work, the link budget is evaluated at 20 mW (13 dBm) of transmitted power to comply with SAR requirements. Application of the Free Space Path Loss (FSPL) formula is included in the evaluation, where 'd' is the distance between the transmitting and receiving antennas [31].

These are actually the standard Friis equations [29], [34], [35] typically used to characterize the wireless communication link. Equation (3) is the free space path loss (FSPL) model, which calculates the signal attenuation over a distance (d), based on frequency (f) and the speed of light (c). Equation (5) is the available power at the receiver. The available power (A_p) at the receiver is determined by adding the transmitted power (P_t) and the antenna gains (G_t) and (G_r), while subtracting the FSPL and noise power density (N_0). Equation (5) is the received power. The received power (R_p) is then calculated using the ratio of energy per bit to noise power spectral density (E_b/N_0), along with the bit rate (B_r) and processing gain (G_d). Equation (6) is the noise power density (N_0), which is derived from Boltzmann's constant (k) and system noise temperature (T_i), which depends on the reference temperature (T_0) and system noise figure (NF). These combined equations enable a thorough assessment of the link margin by considering transmitted power, path loss, antenna gains, bit rate, and noise factors, ensuring the received signal can maintain communication reliability.

$$\text{FSPL} = 20 \times \log\left(4 \times \pi \times d \times\right)\frac{f}{c} \tag{3}$$

$$A_p = P_t + G_t + G_r - \text{FSPL} - N_o \tag{4}$$

$$R_p = \frac{Eb}{No} + 10\log(Br) + G_d \tag{5}$$

$$N_o = 10\log K + 10\log T_i \tag{6}$$

$$T_i = T_o(NF + 1) \tag{7}$$

The parameters of the link budget are outlined in Table 2. An important parameter is the available power, which is defined as the signal-to-noise power density ratio that

the external antenna measures at a certain distance while the endoscopic antenna transmits at a given power. The power required at the receiving end to attain the desired communication rate (called the needed power), is equivalent to the carrier-to-noise ratio required by the communication requirements.

As shown in Fig. 13, the proposed MIMO antenna placed in the small intestine can transmit data at 1 Mbps and 78 Mbps respectively, inside the small intestine at a link margin of 20 dB [36]. The effective communication range of the proposed antenna at 1 Mbps and 78 Mbps data rate is 1.8 m and more than 20 m, respectively as shown in Fig. 13. These findings validate the effectiveness of the endoscopic MIMO antenna for high-speed data transmission at realistic distances, guaranteeing excellent performance in conditions when the human body exhibits considerable signal loss.

FIGURE 13. Link budget for a bit rate of 1 and 78 Mbps between the TX and Rx antennas.

TABLE 2. Link margin parameters.

Transmitter TX	
Parameter	**Value**
Operating Frequency (MHz)	2450
TX antenna Power (dBm/dBW)	13/-17
TX Antenna Gain (dBi)	-28
Receiver RX	
Parameter	**Value**
RX Antenna Gain (dBi)	2.15
Ambient Temperature To(K)	293
Receiver Noise figure (dB)	3.5
Boltzmann constant (K)	1.38×10^{-23}
Noise Power Density (dB /Hz)	-199.95
Signal Quality	
Parameter	**Value**
Bit Rate Br (Mb/s)	1
Bit Error Rate	1×10^{-5}
Ideal Binary phase shift keying	9.6
Fixing Deterioration	2.5

B. CURRENT DISTRIBUTION AND POLARIZATION MECHANISM

The vector current distribution of the proposed design is shown in Fig. 14. The suggested orthogonal port excitation of the Hilbert curve-shaped antenna effectively mitigates mutual coupling, eliminating the need for significant spacing between radiating elements, external decoupling techniques, and a complete ground. The investigation of the surface current distribution aims to comprehend the intensity of coupling between the radiators. Mutual coupling significantly impacts antenna characteristics, including gain, radiation pattern, and bandwidth. Upon activating Port 1, Fig. 14(c) displays the vector current distribution of the antenna system, revealing a quasi-even distribution of current across the stimulated patch. Furthermore, the second antenna is found to be coupled with a very small current, even with only a 1 mm edge-to-edge separation between the two MIMO radiators. The meandering form of Hilbert curve-shaped
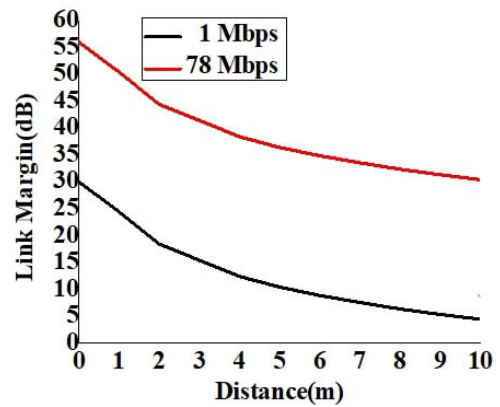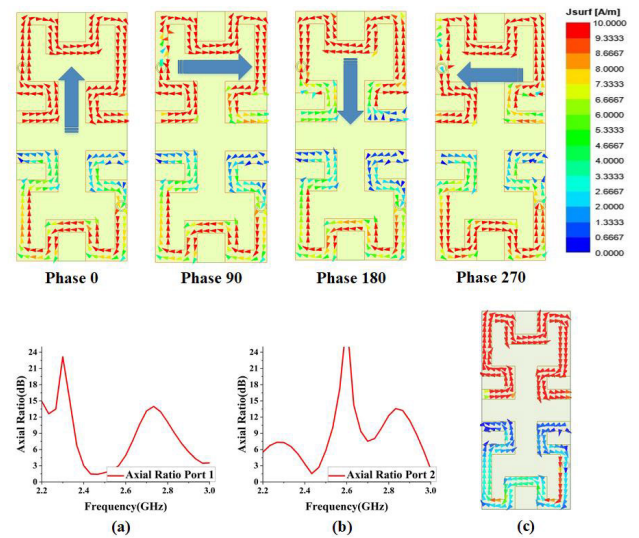

FIGURE 14. (a) axial ratio port 1 (b) axial ratio port 2 (c) vector current distribution.

antennas induces multiple coupling currents, strategically designed to cancel each other out at the nearby antenna port, ensuring high isolation. The figure shows the vector surface current distribution on radiating element-1 of the suggested antenna for the excited Port-1, while Port-2 is matched and terminated. The graph illustrates current flow along the meandering lines in the active radiating components, with each meandering line having a current flowing in the opposite direction from the meandering line. Due to the cancellation of associated fields, very low fields spread to the nearby radiating element. Fig. 14(c) depicts the current distribution of the suggested implanted antenna at the operational frequency indicative of a quarter-wavelength monopole mode [27], [36], [37].

At the assigned resonant frequencies, the circular polarization mechanism of the proposed antenna is clarified. The antenna travels through the whole digestive system while remaining inside the endoscopic capsule and radiating in a circularly polarized manner. Upon achieving a 90-degree phase difference between two equal amplitude mutually

TABLE 3. Comparison of antenna designs.

Ref No.	This Work	[20]	[21]	[22]	[23]	[24]	[25]	[26]
Year	2024	2018	2020	2021	2022	2021	2023	2021
Frequency (MHz)	2450	2450	2450	2450	2450	2450	2450	2450
Isolation (dB)	28.1	15.9	32	37	30.1	28	24	40
Area Size (mm^2)	4×9	18.5×18.5	15×15	10.5×10.5	5×4.2	5.35×6.2	10.8×5.6	6×13
BW (MHz)	250	440	700	210	620	320	148	1100
Antenna Type	Hilbert	EBG	Cubical	Patch	Meander	Meander	Meander	Hilbert
No. of Ports	2	4	4	2	2	2	2	2
ECC	<0.001	<0.0025	<0.1	—	<0.11	<0.1	<0.2	<0.001
DG	9.99	—	—	—	9.9	9.98	9.96	9.98
CP in All Organs	YES	NO	NO	NO	NO	NO	NO	NO

perpendicular electric fields, the suggested endoscopic antenna produces a circularly polarized (CP) wave [14]. In Fig. 14, with its characteristic of rotating the current vector clockwise from the reference feed point in the left corner, the Hilbert loop achieves an AR of less than 3 dB, especially close to the resonant frequency in the large intestine, small intestine, and stomach. The combined effects of different current distributions at different phases (0°, 90°, 180°, 270°) created a phenomenon known as a Circularly Polarized (CP) wave indicated by arrows in Fig. 14 showing the direction of current flow. To improve understanding of the CP operation, a visual representation of the surface current distribution in Fig. 14 is provided at a frequency of 2450 MHz for $\omega \times t = 0°, 90°, 180°, 270°$. The current minima in the Hilbert curve open loop antenna design are arranged so that the current vector rotates clockwise. At both ports, AR is simulated in the small intestine, large intestine, and stomach which is below 3 dB, and bandwidth covers approximately more than 50 per cent of the ISM band. Port 1 and port 2 AR of organs are shown in Fig. 14(a) and Fig. 14(b) respectively. From the graphs in Fig. 14a and 14b, it is evident that the axial ratio bandwidth below 3 dB encompasses nearly the entire ISM band at 2.45 GHz and the black arrow in Fig. 14 indicates the current direction at 0°, 90°, 180°, and 270° phases. At these four phases, the electric field has an orthogonal orientation, showing the CP feature of the proposed design. Thus, AR and current distribution confirm the CP behaviour of the design.

C. MIMO PERFORMANCE

To evaluate MIMO performance matrices, it is crucial to compute various MIMO antenna characteristics such as envelope correlation coefficient (ECC) and diversity gain (DG).

1) ENVELOPE CORRELATION COEFFICIENT

In MIMO antenna systems, the correlation between the envelope of signals received by various antenna components is evaluated using the Envelope Correlation Coefficient (ECC). It measures the degree to which the amplitude variations (envelopes) of signals received by various antennas are similar or correlated. A low correlation between the signals received by the antennas is desirable because designing MIMO antennas with low ECC values is critical for maximizing system performance. In practice, the ECC
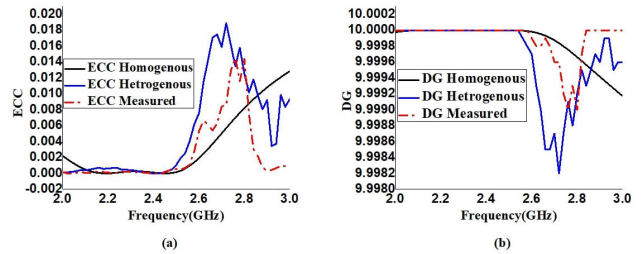

FIGURE 15. ECC and DG of the proposed design.

of a MIMO system is calculated using S-parameters or far-field radiation patterns [36], [38], [39]. In this research, ECC is computed using S Parameters in a homogeneous stomach phantom, heterogenous stomach phantom and minced pork. The plot of ECC values against frequencies is presented in Fig. 15(a) calculated from ECC equation (8) [36], [38], [39].

$$ECC = \frac{\left|\sum_{ij} S_{ij} S_{ij}^*\right|^2}{\left(\sum_{ii} |S_{ii}|^2\right)\left(\sum_{jj} |S_{jj}|^2\right)} \tag{8}$$

where S_{ij} are the respective S-parameters. They account for the interaction between the input and output signals at various ports of a linear electrical network related to one another. As seen in Fig. 15(a), the ECC (homogeneous, heterogeneous and measured) of the suggested MIMO implantable antenna is less than 0.001 in the band of interest.

2) DIVERSITY GAIN (DG)

Diversity gain is a metric that gauges the enhancement in the reliability of a communication system achieved by employing multiple antennas to counteract fading, which refers to fluctuations in the signal strength in wireless channels. A lower ECC value is indicated by a larger directivity gain. This suggests that the fading routes experienced by the antennas are separate, which enables the MIMO system to efficiently reduce the impacts of fading. Contrary to high ECC the diversity gain decreases because the antennas experience similar fading characteristics. Consequently, the system can attain enhanced performance DG quantifies the improvement in the system's performance when faced with fading. A higher diversity gain signifies superior performance in fading channels. The correlation between the ECC value and DG becomes apparent through the relationship given in

equation (9). Thus, as the ECC value decreases, the DG value increases. Therefore, insufficient isolation between antennas leads to a lower DG, as expressed by [36].

$$DG = 10\sqrt{1 - \text{ECC}^2} \qquad (9)$$

The diversity gain has been illustrated in Fig. 15(b). It is observed that the simulated diversity gain (homogeneous and heterogeneous) of the antenna system exceeds 9.99 dB across the entire operating band, reaching 9.98 dB at the 2.45 GHz target band. Similarly, the measured diversity gain of the antenna system remains consistently above 9.90 dB throughout the entire operating band.

Table 3 presents a concise summary of a detailed comparison between the current study and the most recent studies. In comparison to published works, the proposed design has a compact size with high isolation, wide bandwidth, and high CP and MIMO performance. This showcases its significance for its use in implantable devices.

V. CONCLUSION

This study proposed a compact CP MIMO implantable antenna for WCE applications. Our design achieves several excellent key performance characteristics of the WCE antenna, including compactness, gain, bandwidth, circular polarization, high data rate, and low SAR. The orthogonal pin placement makes the isolation between two ports high hence improving decoupling. The Hilbert shape design makes the current flow in such a way as to produce CP performance. ISM bands have been more popular recently because of their wide bandwidth, high data rate, and capacity to support small antenna sizes. Thus, designed for WCE, the proposed antenna achieves a bandwidth of 250 MHz at the 2.45 GHz ISM band. The proposed MIMO antenna offers acceptable gain at the desired frequency. Detailed analysis of the proposed design throughout the digestive tract has shown performance stability within different digestive system organs which is highly desirable for the WCE system. Compared to the state of the art, the proposed design has shown a high compactness, isolation, wide impedance bandwidth, axial ratio bandwidth, ECC and DG which confirms its suitability for WCE applications. Additionally, the evaluated link margin confirms that the proposed MIMO implantable antenna is capable for establishing reliable high data rate link with an external receiver up to significant distances.

ACKNOWLEDGMENT

REFERENCES

[1] S. A. A. Shah and H. Yoo, "Scalp-implantable antenna systems for intracranial pressure monitoring," *IEEE Trans. Antennas Propag.*, vol. 66, no. 4, pp. 2170–2173, Apr. 2018.

[2] A. Kiourti, K. A. Psathas, and K. S. Nikita, "Implantable and ingestible medical devices with wireless telemetry functionalities: A review of current status and challenges," *Bioelectromagnetics*, vol. 35, no. 1, pp. 1–15, Jan. 2014.

[3] S. A. A. Shah, I. A. Shah, S. Hayat, and H. Yoo, "Ultra-miniaturized implantable antenna enabling multiband operation for diverse industrial IoMT devices," *IEEE Trans. Antennas Propag.*, vol. 72, no. 2, pp. 1352–1362, Feb. 2024.

[4] I. A. Shah, M. Zada, S. A. A. Shah, A. Basir, and H. Yoo, "Flexible metasurface-coupled efficient wireless power transfer system for implantable devices," *IEEE Trans. Microw. Theory Techn.*, vol. 72, no. 4, pp. 2534–2547, Apr. 2024.

[5] R. Das and H. Yoo, "A wideband circularly polarized conformal endoscopic antenna system for high-speed data transfer," *IEEE Trans. Antennas Propag.*, vol. 65, no. 6, pp. 2816–2826, Jun. 2017.

[6] A. Basir, M. Zada, Y. Cho, and H. Yoo, "A dual-circular-polarized endoscopic antenna with wideband characteristics and wireless biotelemetric link characterization," *IEEE Trans. Antennas Propag.*, vol. 68, no. 10, pp. 6953–6963, Oct. 2020.

[7] M. Yousaf, I. B. Mabrouk, F. Faisal, M. Zada, Z. Bashir, A. Akram, M. Nedil, and H. Yoo, "Compacted conformal implantable antenna with multitasking capabilities for ingestible capsule endoscope," *IEEE Access*, vol. 8, pp. 157617–157627, 2020.

[8] K. Zhang, C. Liu, X. Liu, H. Cao, Y. Zhang, X. Yang, and H. Guo, "A conformal differentially fed antenna for ingestible capsule system," *IEEE Trans. Antennas Propag.*, vol. 66, no. 4, pp. 1695–1703, Apr. 2018.

[9] Z. Duan, L.-J. Xu, S. Gao, and W. Geyi, "Integrated design of wideband omnidirectional antenna and electronic components for wireless capsule endoscopy systems," *IEEE Access*, vol. 6, pp. 29626–29636, 2018.

[10] M. S. Miah, A. N. Khan, C. Icheln, K. Haneda, and K.-I. Takizawa, "Antenna system design for improved wireless capsule endoscope links at 433 MHz," *IEEE Trans. Antennas Propag.*, vol. 67, no. 4, pp. 2687–2699, Apr. 2019.

[11] P. L. Poshtgol, L. Jichao, S. Soltani, and R. D. Murch, "MIMO antennas for capsule endoscope systems," in *Proc. IEEE Int. Symp. Antennas Propag. (APSURSI)*, Jun. 2016, pp. 1175–1176.

[12] L. Xu, B. Li, M. Zhang, and Y. Bo, "Conformal MIMO loop antenna for ingestible capsule applications," *Electron. Lett.*, vol. 53, no. 23, pp. 1506–1508, Nov. 2017.

[13] A. Basir, Y. Cho, I. A. Shah, S. Hayat, S. Ullah, M. Zada, S. A. A. Shah, and H. Yoo, "Implantable and ingestible antenna systems: From imagination to realization [bioelectromagnetics]," *IEEE Antennas Propag. Mag.*, vol. 65, no. 5, pp. 70–83, Oct. 2023.

[14] S. Hayat, S. A. A. Shah, and H. Yoo, "Miniaturized dual-band circularly polarized implantable antenna for capsule endoscopic system," *IEEE Trans. Antennas Propag.*, vol. 69, no. 4, pp. 1885–1895, Apr. 2021.

[15] S. A. Osman, M. S. El-Gendy, H. M. Elhennawy, and E. A. F. Abdallah, "Reconfigurable flexible inverted-F antenna for wireless capsule endoscopy," *AEU-Int. J. Electron. Commun.*, vol. 155, Oct. 2022, Art. no. 154377.

[16] Z. Xia, H. Li, Z. Lee, S. Xiao, W. Shao, X. Ding, and X. Yang, "A wideband circularly polarized implantable patch antenna for ISM band biomedical applications," *IEEE Trans. Antennas Propag.*, vol. 68, no. 3, pp. 2399–2404, Mar. 2020.

[17] K. Zhang, C. Liu, X. Liu, H. Guo, and X. Yang, "Miniaturized circularly polarized implantable antenna for ISM-band biomedical devices," *Int. J. Antennas Propag.*, vol. 2017, no. 1, pp. 1–9, 2017.

[18] L. V. Tung and C. Seo, "A miniaturized implantable antenna for wireless power transfer and communication in biomedical applications," *J. Electromagn. Eng. Sci.*, vol. 22, no. 4, pp. 440–446, Jul. 2022.

[19] A. Iqbal, M. Al-Hasan, I. B. Mabrouk, and M. Nedil, "A compact implantable MIMO antenna for high-data-rate biotelemetry applications," *IEEE Trans. Antennas Propag.*, vol. 70, no. 1, pp. 631–640, Jan. 2022.

[20] Y. Fan, J. Huang, T. Chang, and X. Liu, "A miniaturized four-element MIMO antenna with EBG for implantable medical devices," *IEEE J. Electromagn., RF Microw. Med. Biol.*, vol. 2, no. 4, pp. 226–233, Dec. 2018.

[21] V. Kaim, B. K. Kanaujia, and K. Rambabu, "Quadrilateral spatial diversity circularly polarized MIMO cubic implantable antenna system for biotelemetry," *IEEE Trans. Antennas Propag.*, vol. 69, no. 3, pp. 1260–1272, Mar. 2021.

[22] M. S. Singh, J. Ghosh, S. Ghosh, and A. Sarkhel, "Miniaturized dual-antenna system for implantable biotelemetry application," *IEEE Antennas Wireless Propag. Lett.*, vol. 20, pp. 1394–1398, 2021.

[23] A. J. Alazemi and A. Iqbal, "A compact and wideband MIMO antenna for high-data-rate biomedical ingestible capsules," *Sci. Rep.*, vol. 12, no. 1, p. 14290, Aug. 2022.

[24] A. J. Alazemi and A. Iqbal, "A high data rate implantable MIMO antenna for deep implanted biomedical devices," *IEEE Trans. Antennas Propag.*, vol. 70, no. 2, pp. 998–1007, Feb. 2022.

[25] S. N. Shah, M. Zada, J. Nasir, S. M. A. Shah, E. Arnieri, and H. Yoo, "Dual-band two-port MIMO antenna for biomedical deep tissue communication: Design, characterization, and performance analysis," *IEEE Access*, vol. 11, pp. 104622–104632, 2023.

[26] B. Biswas, A. Karmakar, and V. Chandra, "Hilbert curve inspired miniaturized MIMO antenna for wireless capsule endoscopy," *AEU-Int. J. Electron. Commun.*, vol. 137, Jul. 2021, Art. no. 153819.

[27] J. Huang and A. Li, "An implantable loop antenna with Hilbert curve structures," *J. Phys., Conf.*, vol. 2209, no. 1, Feb. 2022, Art. no. 012008.

[28] T. Van Nunen, E. Huismans, R. Mestrom, M. Bentum, and H. Visser, "DIY electromagnetic phantoms for biomedical wireless power transfer experiments," in *Proc. IEEE Wireless Power Transf. Conf. (WPTC)*, Jun. 2019, pp. 399–404.

[29] C. A. Balanis, *Antenna Theory: Analysis and Design*. Hoboken, NJ, USA: Wiley, 2016.

[30] M. Ran, M. Ye, and B. Yin, "A dual-band ultra-wideband conformal antenna for WCE," *Prog. Electromagn. Res. M*, vol. 111, p. 101, 2022.

[31] S. A. A. Shah, A. Basir, Y.-H. Lim, and H. Yoo, "A novel efficient wirelessly powered biotelemetric endovascular aortic stent antenna system," *IEEE Trans. Antennas Propag.*, vol. 71, no. 9, pp. 7132–7145, Sep. 2023.

[32] A.-K. Lee, S.-E. Hong, M. Taki, K. Wake, and H. D. Choi, "Comparison of different SAR limits in SAM phantom for mobile phone exposure," in *Proc. Asia–Pacific Microw. Conf. (APMC)*, Nov. 2018, pp. 687–689.

[33] S. A. A. Shah, Y.-H. Lim, and H. Yoo, "A novel development of endovascular aortic stent system featuring promising antenna characteristics," *IEEE Trans. Antennas Propag.*, vol. 70, no. 3, pp. 2214–2222, Mar. 2022.

[34] A. Lamkaddem, A. E. Yousfi, V. González-Posadas, and D. Segovia-Vargas, "Miniaturized dual band implantable antenna for implanted biomedical devices," *IEEE Access*, vol. 12, pp. 15026–15036, 2024.

[35] A. Lamkaddem, A. E. Yousfi, K. A. Abdalmalak, V. G. Posadas, and D. Segovia-Vargas, "Circularly polarized miniaturized implantable antenna for leadless pacemaker devices," *IEEE Trans. Antennas Propag.*, vol. 70, no. 8, pp. 6423–6432, Aug. 2022.

[36] S. M. A. Shah, M. Zada, J. Nasir, O. Owais, A. Iqbal, and H. Yoo, "Miniaturized four-port MIMO implantable antenna for high-data-rate wireless-capsule-endoscopy applications," *IEEE Trans. Antennas Propag.*, vol. 71, no. 4, pp. 3123–3133, Apr. 2023.

[37] Y.-F. Cheng and K.-K.-M. Cheng, "Decoupling of two-element printed-dipole antenna array by optimal meandering design," *IEEE Trans. Antennas Propag.*, vol. 68, no. 11, pp. 7328–7338, Nov. 2020.

[38] K. Raheel, A. W. Ahmad, S. Khan, S. A. A. Shah, I. A. Shah, and M. Dalarsson, "Design and performance evaluation of orthogonally polarized corporate feed MIMO antenna array for next-generation communication system," *IEEE Access*, vol. 12, pp. 30382–30397, 2024.

[39] H. Sarfraz, S. Khan, N. Khan, N. Gohar, S. A. A. Shah, J. Nasir, and M. Dalarsson, "Next-generation multiband wireless systems: A compact CSSR-based MIMO dielectric resonator antenna approach," *IEEE Access*, vol. 12, pp. 4910–4924, 2024.

with COMSATS University Islamabad. He is also an Antenna Design Engineer specializing in advanced antennas for biomedical devices, 5G technologies, and UHF frequency applications. His research interests include machine-learning-assisted antennas implantable antennas, MIMO antennas, dielectric resonator antennas, wireless power transfer, and circularly polarized antennas.

SYED AHSON ALI SHAH (Member, IEEE) received the B.Sc. degree in telecommunication engineering from the University of Engineering and Technology, Mardan, Pakistan, in 2015, and the M.S. degree leading to the Ph.D. degree in electronic engineering from Hanyang University, Seoul, South Korea, in 2022. He was a Postdoctoral Researcher with Hanyang University until 2023. Since then, he has been with Gwangju Institute of Science and Technology. His research interests include free-space antennas for wireless communications, implantable antennas and systems, implant safety, wireless power transfer systems, sensor-integrated biotelemetric stents, reconfigurable antennas, metamaterial-based antenna systems, and 5G antenna development. He was a recipient of the IETE MN SAHA Memorial Award; the Gold Medal for Best Application-Oriented Paper, in 2018; and the Bronze Paper Award at the IEEE Student Paper Contest, Seoul, in 2019, 2021, and 2022. He also won the 3rd Best Student Paper Award, in 2021, arranged by the Korean Institute of Electromagnetic Engineering and Science (KIEES). His Ph.D. thesis has been recognized as one of the excellent dissertations and received the Best Ph.D. Thesis Award in overall university and the only on the Electronic Engineering Department.

SHAHID KHAN was born in Landikotal, Pakistan, in 1986. He received the B.S. degree in telecommunication engineering from the University of Engineering and Technology, Peshawar, Pakistan, the M.S. degree in satellite navigation and related applications from Politecnico de Torino, Italy, in 2011, and the Ph.D. degree from the University of Lorraine, France, in 2021. He was a Visiting Fellow at the 5G Innovation Center, University of Surrey. Currently, he is working as a Research Assistant Professor with the Faculty of Electronics, Telecommunications and Informatics, Gdánsk University of Technology, Poland. His research interests include development of circularly polarized phased array DRAs for satellite application, implantable antennas, and reconfigurable dielectric resonator antenna for different wireless applications.

IZAZ ALI SHAH received the B.Sc. degree in telecommunication engineering from the University of Engineering and Technology, Mardan, Pakistan, in 2016, and the Ph.D. degree in electronic engineering from Hanyang University, Seoul, South Korea, in 2023. Since February 2023, he has been a Postdoctoral Researcher with the Applied Bioelectronics Laboratory (ABL), Hanyang University. His current research interests include implantable antennas and devices, wireless power transfer to electric vehicles, portable devices, implantable devices, metasurfaces, and implant safety. He was a recipient of a fully funded scholarship awarded by the Prime Minister's National ICT Research and Development Fund throughout the bachelor's degree program. He was also a recipient of the Best Student Paper Competition Award by Korean Institute of Electromagnetic Engineering, in 2018 and 2020. He is serving as a Reviewer for IEEE TRANSACTIONS ON ANTENNA AND PROPAGATION, IEEE TRANSACTIONS ON INDUSTRIAL ELECTRONICS, and Elsevier journals.

SYED MISBAH UN NOOR was born in Peshawar, Pakistan, in 1991. He received the B.S. degree in electrical engineering from the Department of Electrical Engineering, COMSATS University Islamabad, Abbottabad Campus, in 2014, and the M.S. degree in electrical engineering from the Department of Electrical Engineering, University of Engineering and Technology, Peshawar, in 2019. He is currently pursuing the Ph.D. degree in electrical engineering

JAMAL NASIR was born in Khyber Pakhtunkhwa, Pakistan, in 1983. He received the M.Sc. degree in mobile and satellite communication from the University of Bradford, Bradford, U.K., in 2007, and the Ph.D. degree in electrical engineering from Universiti Teknologi Malaysia, Johor Bahru, Malaysia, in 2017. He is currently an Assistant Professor with the Department of Electrical Engineering, COMSATS University Islamabad, Abbottabad Campus, Khyber Pakhtunkhwa. His research interests include SIW-based passive components and arrays, metamaterials, smart antennas, mutual coupling analysis, MIMO antennas, dielectric resonator antennas, UWB antennas, and wearable antennas.

SLAWOMIR KOZIEL (Fellow, IEEE) received the M.Sc. and Ph.D. degrees in electronic engineering from Gdańsk University of Technology, Poland, in 1995 and 2000, respectively, and the M.Sc. degree in theoretical physics and the M.Sc. and Ph.D. degrees in mathematics from the University of Gdańsk, Poland, in 2000, 2002, and 2003, respectively. He is currently a Professor with the School of Science and Engineering, Reykjavik University, Iceland. His research interests include CAD and modeling of microwave and antenna structures, simulation-driven design, surrogate-based optimization, space mapping, circuit theory, analog signal processing, evolutionary computation, and numerical analysis.

• • •

SALAHUDDIN KHAN is currently an Associate Professor with King Saud University. He is specialized in design, modeling, and simulation which can be extended to various fields of electronics, electromagnetic, and power systems, such as development of algorithms, realization of antenna devices, and power plant secondary systems. The above research lines have produced many research projects and publications. He has also contributed U.S. patent.